Frontiers of Information Technology & Electronic Engineering
www.jzus.zju.edu.cn; engineering.cae.cn; www.springerlink.com
ISSN 2095-9184 (print); ISSN 2095-9230 (online)
E-mail: jzus@zju.edu.cn

Supplementary materials for

Lakshminarayana JANJANAM, Suman Kumar SAHA, Rajib KAR, 2024. Enhancing modelling accuracy of cascaded spline adaptive filters using the remora optimisation algorithm: application to real-time systems. *Front Inform Technol Electron Eng*, 25(11):1515-1535. https://doi.org/10.1631/FITEE.2300817

1 A pictorial representation of the mathematical analysis HW-SAF modelling

The pictorial representation of the mathematical analysis of the HW-SAF modelling is depicted in Fig. S1.

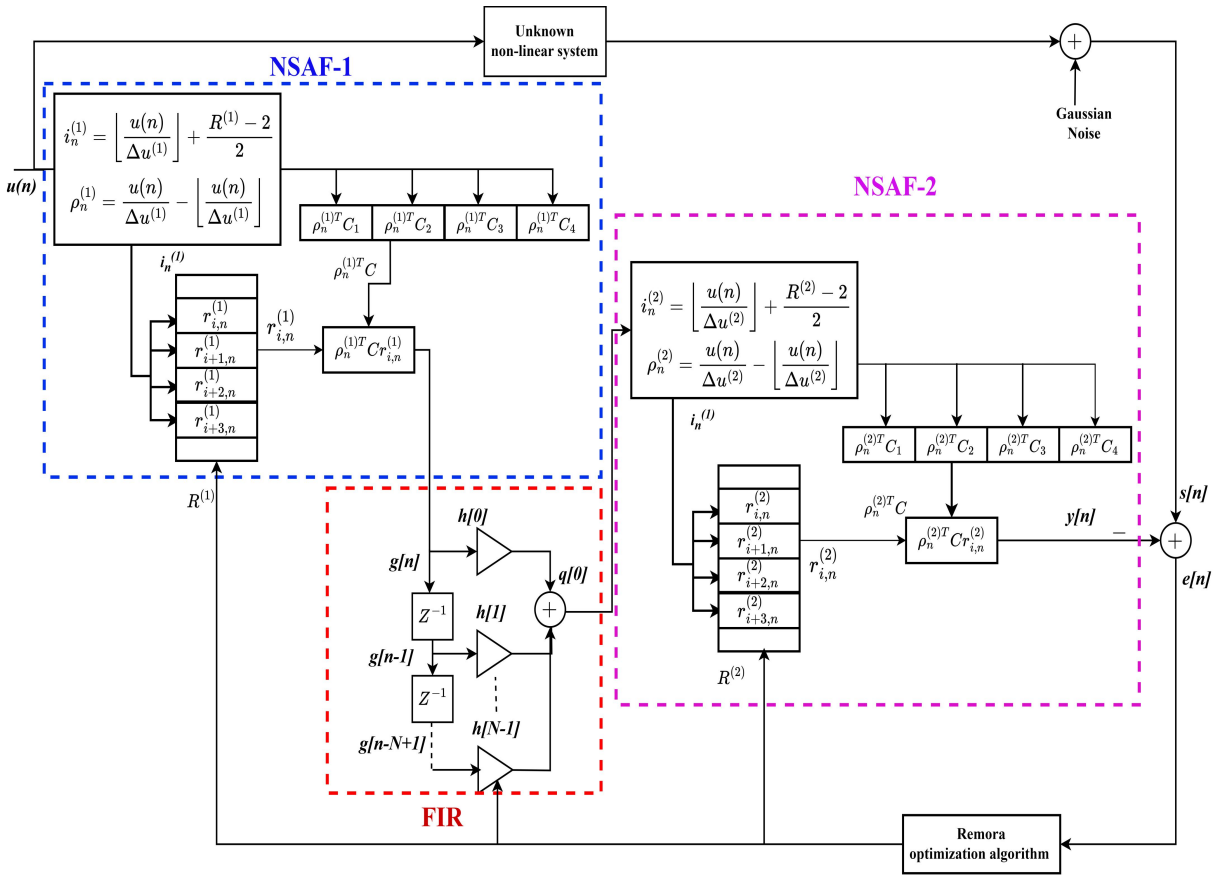

Fig. S1 Implementation of the proposed ROA-based HW-SAF

2 The pseudocode of the proposed ROA-based CSAF design

The pseudocode of the proposed ROA-based CSAF design is presented in Table S1.

Table S1 Pseudocode of the proposed ROA-based CSAF design

Input: Number of populations (NP), maximum iteration number (T), remora factor (V), and set current iteration (t)=1
Output: Best search agent B_{best} and the optimised WH-SAF or HW-SAF parameters it carries
Randomise NP populations using Eq. (11)
while $t<T$ **do**
Evaluate the fitness of each remora by Eq. (6) or (10) and save the lowest fitness position in B_{best}
Amend if any search agent moves beyond the search space
Calculate β , γ , and ξ by Eqs. (14)-(16)
For each remora indexed by k **do**
If $H(k)$=0 **then**
Amend whales position by Eq. (17)
Else if $H(k)$=1 **then**
Amend sailfishes position by Eq. (18)
End if
Perform experience attack phase using Eq. (19)
If fitness ($B_{att}(t)$)>fitness ($B_k(t)$) **then**
Update B_{att}(t)=$B_k(t)$ and $H(k)$=round(rand) for host replacement
Else
Amend the location of remora by Eq. (20)
End if
End while
Report B_{best}

3 Justification for the choice of common control parameter values

In order to select values of common control parameters (lb, ub, NP, and T values), the authors have used the strategy described in Janjanam et al. (2022a) and Nayak et al. (2019). Three different boundary sets, namely, (lb=-3, ub=3), (lb=-10, ub=10), and (lb=-50, ub=50), have been considered. For each set of values, the authors have performed 100 independent simulation suns on system 1 with noise variance level σ^2 =0.001^2 using the proposed ROA-based design scheme. The obtained average fitness value for the set (lb=-10, ub=10) is 3.48E-13. However, a low-quality solution (average fitness of 5.94E-08) is obtained when the search boundary is limited to (lb=-3, ub=3). On the other hand, a suboptimal solution (average fitness of 6.77E-11) is achieved when the search topography diversifies to (lb=-50, ub=50). Hence, in this work, the authors have fixed lb and ub values to -10 and 10, respectively.

Properly selecting population size (NP) is also essential because it influences the quality of results and the exploration efficacy. Moreover, the selection NP value varies based on the problem, and there is no specific rule for setting the NP value. If a smaller NP value is chosen, then the problem search space is not entirely explored, which results in a suboptimal solution. On the other hand, the selection of a more considerable NP value leads to a higher CC. Therefore, in this work, the authors have performed rigorous simulations on system 1 by selecting three different NP values, 15, 25, and 50. The obtained fitness function results (mean of 100 independent runs) for NP equal to 15, 25, and 50 are 8.34E-08, 3.48E-13, and 9.67E-14, respectively. Based on these results, the authors obtained the best result (fitness of 9.67E-14) when the NP value of 50 was chosen. However, the CC of the algorithm is high. Hence, to maintain a good balance between CC and solution quality, the authors have

selected an NP value equal to 25 for all chosen algorithms for modelling all systems. Due to the large problem dimension, the maximum number of iterations (T) is 1000.

4 Parameter convergence profiles of system 2 using the ROA method

Parameter convergence profiles of system 2 using the ROA method is shown in Fig. S2.

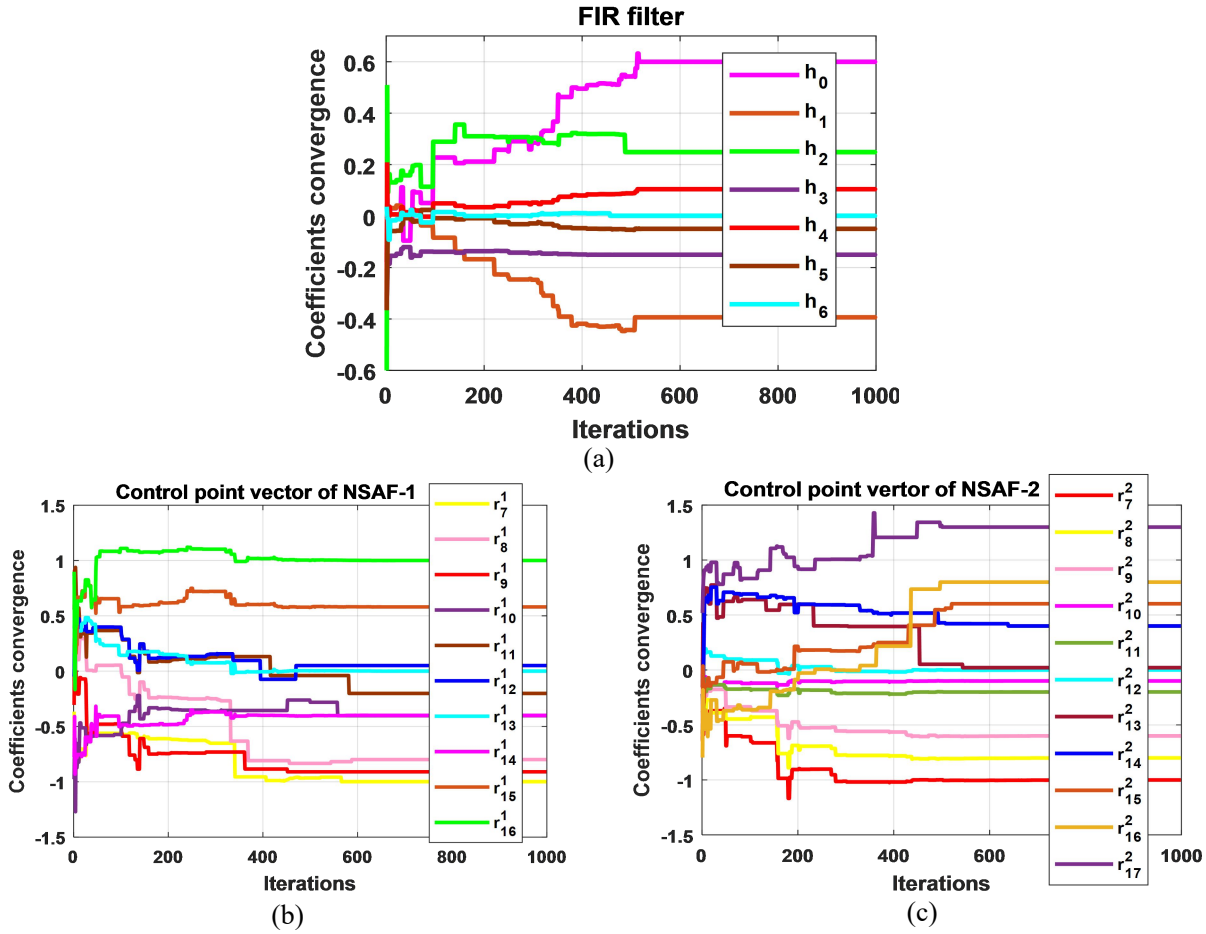

Fig. S2 Parameter convergence profiles of system 2 for the best run of ROA technique: (a) FIR filter coefficients; (b) NSAF-1 spline control points; (c) NSAF-2 spline control points

5 AE metric results for system 2 using the ROA, MVO, BSO, and DE algorithms under different noise variance levels

AE metric results for system 2 by using the ROA, MVO, BSO, and DE algorithms under different noise variance levels are shown in Fig. S3.

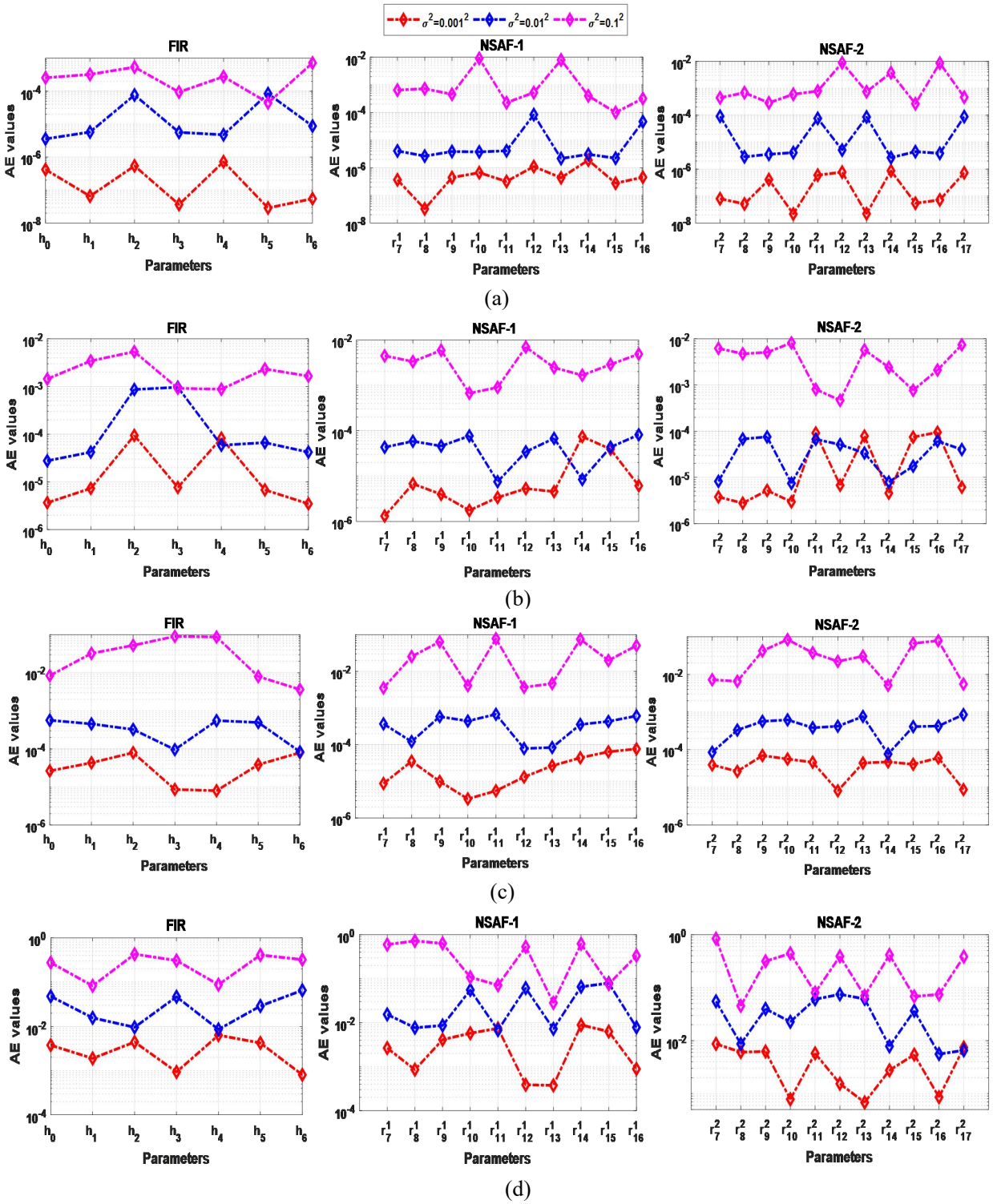

Fig. S3 AE metric results for system 2 using the ROA, MVO, BSO, and DE algorithms under different noise variance levels: (a) ROA; (b) MVO; (c) BSO; (d) DE

6 Comparison of the performance of the techniques used for system 2 based on various performance indices

Comparison of the performance of the employed techniques for systems 2 for various performance indexes is reported in Table S2.

Table S2 Comparison of various performance indices for the employed techniques used for system 2

System	Method	Noise (σ^2)	Accuracy measures						
			MAE	RMSD	MWD	TIC	Fitness (J_1/J_2)	CT(s)	Iteration at the best fitness
2	ROA	0.001^2	7.44E-08	9.65E-09	4.32E-08	1.22E-07	5.40E-13	0.561	454
		0.01^2	3.12E-06	2.11E-08	7.01E-07	6.42E-06	3.54E-11	0.587	414
		0.1^2	6.41E-04	4.21E-06	9.43E-06	2.76E-05	8.97E-07	0.570	287
	MVO	0.001^2	3.22E-07	9.23E-08	8.34E-07	7.43E-07	5.83E-11	0.733	542
		0.01^2	2.98E-05	7.56E-06	8.44E-06	9.27E-05	8.76E-09	0.721	440
		0.1^2	7.11E-03	8.43E-05	9.21E-04	3.54E-04	5.67E-07	0.729	294
	BSO	0.001^2	6.55E-05	6.01E-06	3.33E-05	3.89E-05	4.27E-09	0.987	552
		0.01^2	7.85E-04	6.87E-05	3.76E-03	5.76E-04	2.71E-08	0.933	455
		0.1^2	3.77E-02	2.34E-03	5.89E-02	3.21E-03	6.73E-07	0.951	335
	DE	0.001^2	6.55E-03	4.11E-03	3.76E-04	5.98E-03	6.77E-07	1.113	382
		0.01^2	7.85E-02	6.82E-02	9.27E-03	2.65E-02	7.32E-05	1.022	332
		0.1^2	3.77E-01	1.32E-02	7.54E-02	9.43E-02	5.47E-03	1.089	213

7 Fitness convergence profiles for system 2

In case of system 2 modelling, it can be noticed from Fig. S4 that the three noise variance levels σ^2 =0.001^2, 0.01^2, and 0.1^2 yield the optimum fitness orders of 10^{-13}, 10^{-11}, and 10^{-06} after completion of 454, 414, and 287 iterations in the case of ROA-based method respectively, 10^{-10}, 10^{-00}, and 10^{-06}after 542, 440, and 294 iterations in the case of MVO method respectively, 10^{-09}, 10^{-08}, and 10^{-06} after 552, 455, and 335 iterations in the case of BSO method respectively, 10^{-06}, 10^{-04}, and 10^{-03} after 382, 332, and 213 iterations in the case of DE method respectively.

8 Percentage improvement resulting from the use of the proposed algorithm over others for systems 1 and 2

The improvement of the proposed ROA-based technique over other chosen algorithms for systems 1 and 2 in terms of different metrics under the noise variance level σ^2 =0.001^2 is drawn in Fig. S5. In case of system 1, it can be observed from Fig. S5 that the achieved improvement using ROA over MVO, BSO, and DE is 88.8421%, 98.3145%, and 99.9518% respectively for MAE, 97.3089%, 99.6303%, and 99.9997% respectively for RMSD, 97.4955%, 99.9780%, and 99.9959% respectively for MWE metric, 91.2055%, 99.1748%, and

99.9991% respectively for TIC, and finally 99.2686%, 99.9990%, and 99.9999% respectively for the fitness metric. It can be inferred from Fig. S5 that the improvement of ROA-based approach for system 2 as compared with the other counterpart approaches, namely, MVO, BSO, and DE, is 76.8944%, 99.8864%, and 99.9989% respectively for MAE metric, 89.5450%, 99.8394%, and 99.9998% respectively for RMSD metric, 94.8201%, 99.8703%, and 99.9885% respectively for MWD metric, 83.5801%, 99.6864%, and 99.9980% respectively for TIC metric, and 99.0459%, 99.9874%, and 99.9999% respectively for fitness metric.

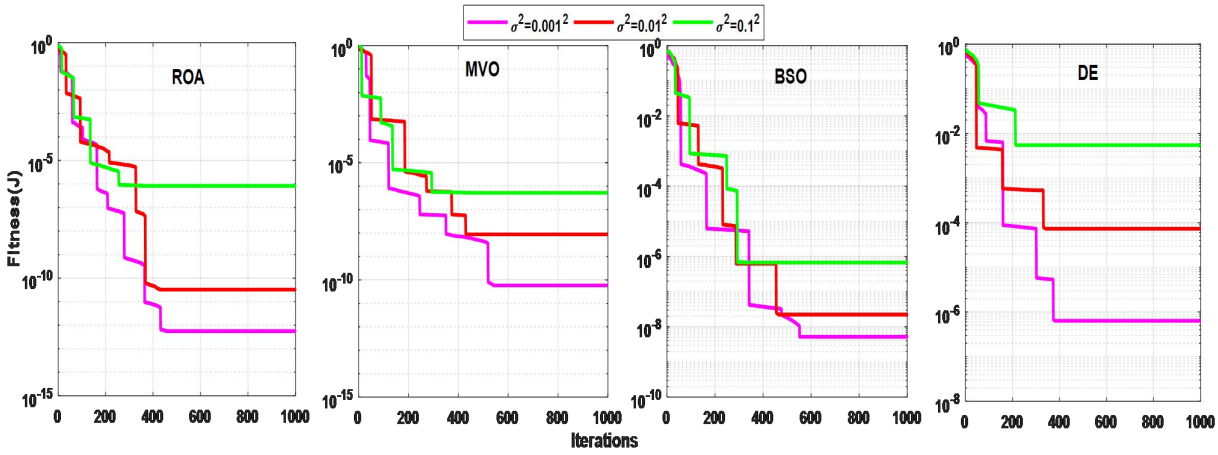

Fig. S4 Fitness convergence profiles for system 2 using the ROA, MVO, BSO, and DE algorithms under different noise levels

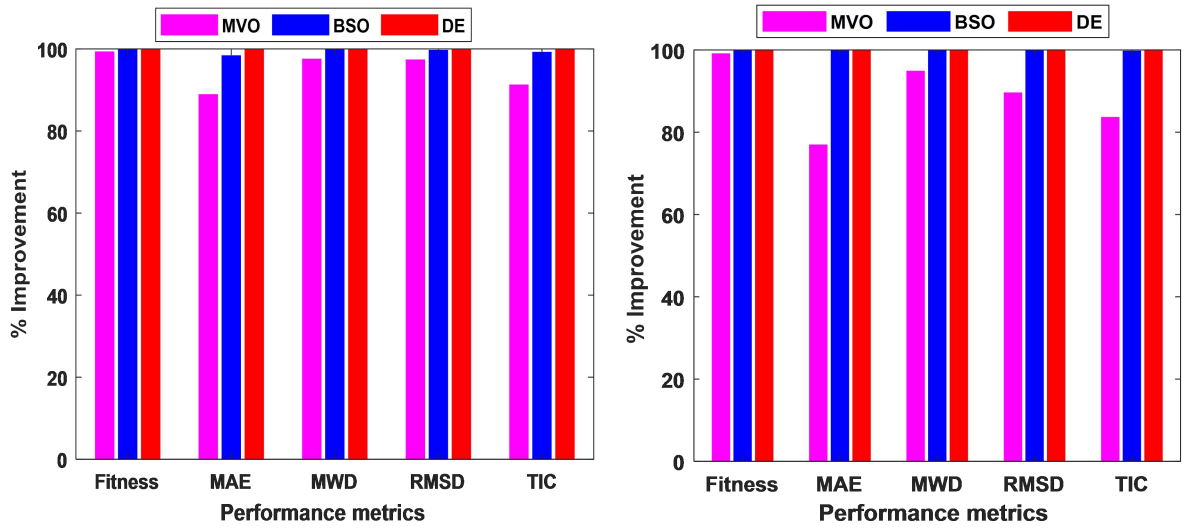

(a) (b)

Fig. S5 Improvement of the proposed ROA-based design compared to MVO-, BSO-, and DE-based designs for systems 1 and 2 with the noise level of σ^2=0.001^2 in terms of different metrics: (a) system 1; (b) system 2

9 Statistical results of the estimated parameters of system 2

Statistical results of the estimated parameters of system 2 are shown in Table S3.

Table S3 Statistical results of the estimated parameters of system 2 using the chosen algorithms under the noise level of $\sigma^2 = 0.001^2$

Method	Metric	FIR filter			NSAF-1				NSAF-2			
		h_0	h_3	h_6	$r_7^{(1)}$	$r_{10}^{(1)}$	$r_{13}^{(1)}$	$r_{16}^{(1)}$	$r_7^{(2)}$	$r_{10}^{(2)}$	$r_{13}^{(2)}$	$r_{16}^{(2)}$
		0.6	-0.15	0.001	-1.0	-0.40	0.0	1.0	-1.0	-0.10	0.02	0.8
		h_1	h_4		$r_8^{(1)}$	$r_{11}^{(1)}$	$r_{14}^{(1)}$		$r_8^{(2)}$	$r_{11}^{(2)}$	$r_{14}^{(2)}$	$r_{17}^{(2)}$
		-0.4	0.1		-0.8	-0.20	-0.40		-0.8	-0.20	0.40	1.35
		h_2	h_5		$r_9^{(1)}$	$r_{12}^{(1)}$	$r_{15}^{(1)}$		$r_9^{(2)}$	$r_{12}^{(2)}$	$r_{15}^{(2)}$	
		0.25	-0.05		-0.91	0.05	0.58		-0.60	0.0	0.60	
ROA	Best	0.600	-0.149	0.001	-1.000	-0.399	0.000	1.000	-0.999	-0.101	0.019	0.799
		-0.400	0.100	N/A	-0.801	-0.199	-0.401	N/A	-0.798	-0.201	0.399	1.350
		0.249	-0.050	N/A	-0.910	0.050	0.579	N/A	-0.599	0.000	0.601	N/A
	Mean	0.601	-0.150	0.001	-1.000	-0.400	0.000	1.000	-0.998	-0.100	0.019	0.801
		-0.400	0.101	N/A	-0.800	-0.199	-0.400	N/A	-0.799	-0.201	0.400	1.349
		0.250	-0.05	N/A	-0.910	0.049	0.578	N/A	-0.600	0.000	0.599	N/A
	Worst	0.600	-0.149	0.001	-1.001	-0.399	0.000	1.000	-0.997	-0.099	0.019	0.800
		-0.399	0.009	N/A	-0.801	-0.198	-0.399	N/A	-0.798	-0.199	0.398	1.348
		0.250	-0.050	N/A	-0.909	0.049	0.479	N/A	-0.601	0.000	0.598	N/A
MVO	Best	0.598	-0.148	0.001	-0.993	-0.391	0.001	0.972	-0.979	-0.091	0.018	0.792
		-0.399	0.099	N/A	-0.793	-0.191	-0.392	N/A	-0.767	-0.192	0.379	1.321
		0.249	-0.049	N/A	-0.898	0.046	0.572	N/A	-0.572	0.001	0.581	N/A
	Mean	0.598	-0.148	0.001	-0.994	-0.390	0.001	0.973	-0.978	-0.090	0.018	0.793
		-0.397	0.095	N/A	-0.795	-0.192	-0.391	N/A	-0.766	-0.193	0.380	1.322
		0.249	-0.048	N/A	-0.897	0.046	0.571	N/A	-0.572	0.0011	0.580	N/A
	Worst	0.596	-0.147	0.001	-0.995	-0.390	0.001	0.972	-0.977	-0.090	0.018	0.791
		-0.396	0.102	N/A	-0.793	-0.191	-0.390	N/A	-0.765	-0.194	0.381	1.321
		0.248	-0.047	N/A	-0.894	0.046	0.570	N/A	-0.571	0.0010	0.580	N/A
BSO	Best	0.589	-0.144	9E-04	-0.937	-0.365	0.002	0.889	-0.905	-0.082	0.017	0.702
		-0.396	0.093	N/A	-0.742	-0.159	-0.346	N/A	-0.697	-0.185	0.293	1.272
		0.246	-0.043	N/A	-0.869	0.041	0.525	N/A	-0.536	0.002	0.490	N/A
	Mean	0.589	-0.144	8E-04	-0.934	-0.367	0.002	0.889	-0.906	-0.083	0.018	0.701
		-0.395	0.093	N/A	-0.744	-0.160	-0.345	N/A	-0.699	-0.187	0.294	1.274
		0.241	-0.044	N/A	-0.866	0.040	0.527	N/A	-0.535	0.002	0.491	N/A
	Worst	0.589	-0.144	8E-04	-0.933	-0.365	0.002	0.887	-0.905	-0.081	0.018	0.701
		-0.395	0.093	N/A	-0.742	-0.160	-0.343	N/A	-0.696	-0.184	0.293	1.270
		0.246	-0.044	N/A	-0.865	0.040	0.52	N/A	-0.534	0.002	0.490	N/A
DE												
	Best	0.576	-0.141	7E-04	-0.907	-0.305	0.003	0.795	-0.833	-0.075	0.012	0.682
		-0.386	0.092	N/A	-0.696	-0.129	-0.316	N/A	-0.601	-0.171	0.237	1.215
		0.223	-0.039	N/A	-0.793	0.038	0.485	N/A	-0.443	0.003	0.444	N/A
	Mean	0.576	-0.141	7E-04	-0.905	-0.307	0.003	0.796	-0.834	-0.076	0.013	0.682
		-0.386	0.092	N/A	-0.698	-0.129	-0.315	N/A	-0.600	-0.170	0.238	1.217
		0.223	-0.040	N/A	-0.794	0.036	0.487	N/A	-0.442	0.003	0.446	N/A
	Worst	0.5754	-0.140	7E-04	-0.904	-0.305	0.003	0.794	-0.832	-0.075	0.011	0.681
		-0.3858	0.091	N/A	-0.696	-0.126	-0.314	N/A	-0.600	-0.170	0.237	1.215
		0.2228	-0.039	N/A	-0.795	0.035	0.485	N/A	-0.440	0.003	0.445	N/A

N/A: Not applicable

10 Statistical analysis of the global metric results for system 2

Statistical analysis of the global metric results for system 2 is shown in Table S4.

Table S4 Statistical analysis of the global metric results for system 2 using the chosen algorithms under different noise levels

System	Method	Noise (σ^2)	Global measures							
			GMAE		GRMSD		GTIC		GFIT	
			Mean	STD	Mean	STD	Mean	STD	Mean	STD
2	ROA	0.001^2	8.22E-08	3.67E-09	8.76E-09	1.45E-10	3.33E-07	2.27E-10	3.48E-13	5.76E-14
		0.01^2	2.17E-06	7.54E-06	5.65E-08	5.77E-09	5.25E-06	4.12E-08	5.89E-11	2.21E-11
		0.1^2	8.76E-04	3.21E-05	3.79E-06	2.93E-06	3.78E-05	6.85E-06	6.12E-07	5.69E-10
	MVO	0.001^2	5.43E-06	4.79E-06	4.43E-07	4.78E-09	4.41E-07	2.94E-08	2.54E-12	3.28E-13
		0.01^2	3.98E-05	3.23E-05	2.75E-05	6.56E-07	6.78E-05	4.33E-07	7.15E-10	5.46E-11
		0.1^2	9.87E-04	7.65E-05	5.49E-04	4.71E-05	5.87E-03	3.56E-05	8.21E-08	1.29E-09
	BSO	0.001^2	2.98E-05	2.36E-06	8.65E-05	6.33E-07	4.69E-05	2.82E-06	5.33E-07	4.86E-08
		0.01^2	6.32E-03	4.54E-05	6.15E-04	4.55E-06	7.53E-04	4.75E-05	4.78E-06	3.51E-07
		0.1^2	8.23E-02	5.98E-03	2.68E-03	2.51E-05	6.68E-03	3.95E-03	5.53E-05	4.73E-06
	DE	0.001^2	6.93E-03	8.32E-05	3.64E-03	2.88E-05	7.39E-03	4.55E-04	9.29E-07	2.83E-05
		0.01^2	2.75E-02	3.57E-04	5.73E-02	6.54E-04	6.73E-02	2.94E-03	8.88E-05	5.09E-05
		0.1^2	6.89E-01	4.13E-02	4.89E-02	9.65E-02	1.96E-02	7.14E-02	3.16E-03	7.30E-03

11 Fitness metric results from 100 independent runs of the algorithms used for system 2

Fitness metric results on 100 independent runs of the employed algorithms for system 2 are shown in Fig. S6.

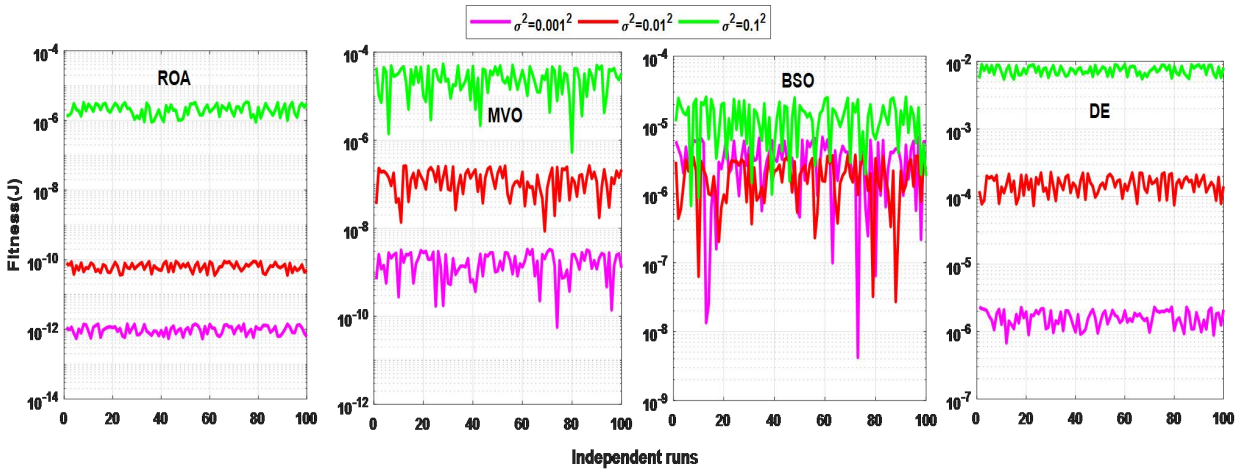

Fig. S6 Independent run results of fitness metric for system 2 using the considered algorithms under different noise levels

12 Holm's consistency test

The consistency of the ROA method over MVO, BSO, and DE algorithms for the design of CSAFs is verified using Holm's test (Shadravan et al., 2019). To accomplish this test between pair-wise algorithms (ROA/MVO, ROA/BSO, and ROA/ DE), the authors have collected different fitness metric values by simulating each algorithm multiple times. The mechanism to implement this test was elaborately described (Holm, 1979; Braik et al., 2022). Let us consider that H_0 (null hypothesis) indicates no noticeable difference between the fitness metric values of both algorithms achieved through different runs. In contrast, H_a (alternate hypothesis) represents a noticeable difference between the fitness samples. Also, consider α which denotes the significance level whose value equals 0.05.

The results of Holm's test for each pair of algorithms for systems 1 and 2 under various noisy conditions (σ^2=0.001^2, 0.01^2, and 0.1^2) are listed in Table S5. In Table S5, τ represents the algorithm number assigned after sorting algorithms' p-values in descending order. It can be discerned from Table S5 that the achieved p-values of each pair-wise scheme are less than the α/τ values except for the ROA/DE pair. Hence, hypothesis H_0 is rejected for BSO and MVO. However, it is accepted for DE. Rejection of the null hypothesis infers that the ROA derives more consistent results in each run than MOA and BSO. Additionally, the DE algorithm shows consistent performance but yields poor estimation results.

Table S5 Holm's test for the employed algorithms for systems 1 and 2

System	ROA vs.	z-value at noise level (σ^2)			p-value at noise level (σ^2)			τ	α/τ	Hypothesis (H_0)
		0.001^2	0.01^2	0.1^2	0.001^2	0.01^2	0.1^2			
1	BSO	6.5573	8.8892	8.5216	4.5562E-08	5.7785E-09	7.5124E-08	3	0.0166	Reject
	MVO	5.6539	4.3357	7.3834	7.8853E-06	8.4967E-06	4.3328E-06	2	0.025	Reject
	DE	1.3317	1.8471	2.5781	0.1657	0.1845	0.2101	1	0.05	Accept
2	BSO	5.3284	7.5543	9.5553	7.6572E-07	5.3749E-07	6.5894E-08	3	0.0166	Reject
	MVO	3.6745	5.7693	6.8783	6.7543E-04	4.4365E-05	3.7662E-06	2	0.025	Reject
	DE	0.8452	2.114	2.5541	0.0954	0.1562	0.1976	1	0.05	Accept

13 Proof of O(MOA)=$O(F(x))O$(NP·($T\varpi$+1))

To evaluate the computational complexity (CC) of the employed metaheuristic optimization algorithm (MOA), initialise the number of populations or candidate solution (NP) and its CC $O(\mathrm{NP})$. Next, the complexity of assessing fitness function is $O(F(x))$, where $F(x)$ denotes the fitness function of the chosen problem. To improve the quality of optimal solutions, each employed MOA performs the exploration (global search) and exploitation (local search) operations. Hence, the CC of the exploration stage is $O(\mathrm{NP}\times T\times\varpi)$ and the exploitation stage is represented as $O(\mathrm{NP}\times T\times\varpi)$, where T is the maximum iteration number and ϖ is the dimension of the problem. The overall CC of each employed MOA-based design scheme is represented as follows (Janjanam et al., 2022c; Jia et al., 2021; Yadav et al., 2023):

$$O(\mathrm{MOA}) = O(\mathrm{Fitnessfunction})\times\Big(O\Big(T\times\big(O(\mathrm{Initialization})+O(\mathrm{Exploration})+O(\mathrm{Exploitation})\big)\Big)\Big),$$

$$O(\mathrm{MOA}) = O(F(x))\times\Big(O\Big(T\times\big(O(\mathrm{NP})+O(\mathrm{NP}\times T\times\varpi)+O(\mathrm{NP}\times T\times\varpi)\big)\Big)\Big),$$

$$O(\mathrm{MOA}) = O(F(x))\times O\Big(\mathrm{NP}\times\big(T\varpi+1\big)\Big).$$

14 Basic details of the coupled electric drive system

The basic snapshot of the laboratory setup of the coupled electric drives (Wigren et al., 2013) is shown in Fig. S7a. This system has two electric motors that drive a pulley through a flexible belt. A spring is used to hold the pulley, creating slight dynamic damping. The drive control (input) is symmetric at about zero; hence, clockwise and anticlockwise movements are possible. As seen in Fig. S7a, the belt's angular speed (output) is measured using the pulse generator. Further details of this system are available in Wigren et al. (2013). To model this system, the authors have taken two publicly accessible real data sets (drive-1 and drive-2) from Wigren et al. (2013). Each drive data carries 500 input/output (I/O) data samples with a sampling period of 20 ms. The authors have used 400 I/O samples for estimation and 100 I/O samples to validate the system. The I/O data samples of drive-1 and drive-2 are shown in Figs. S7b and S7c, respectively.

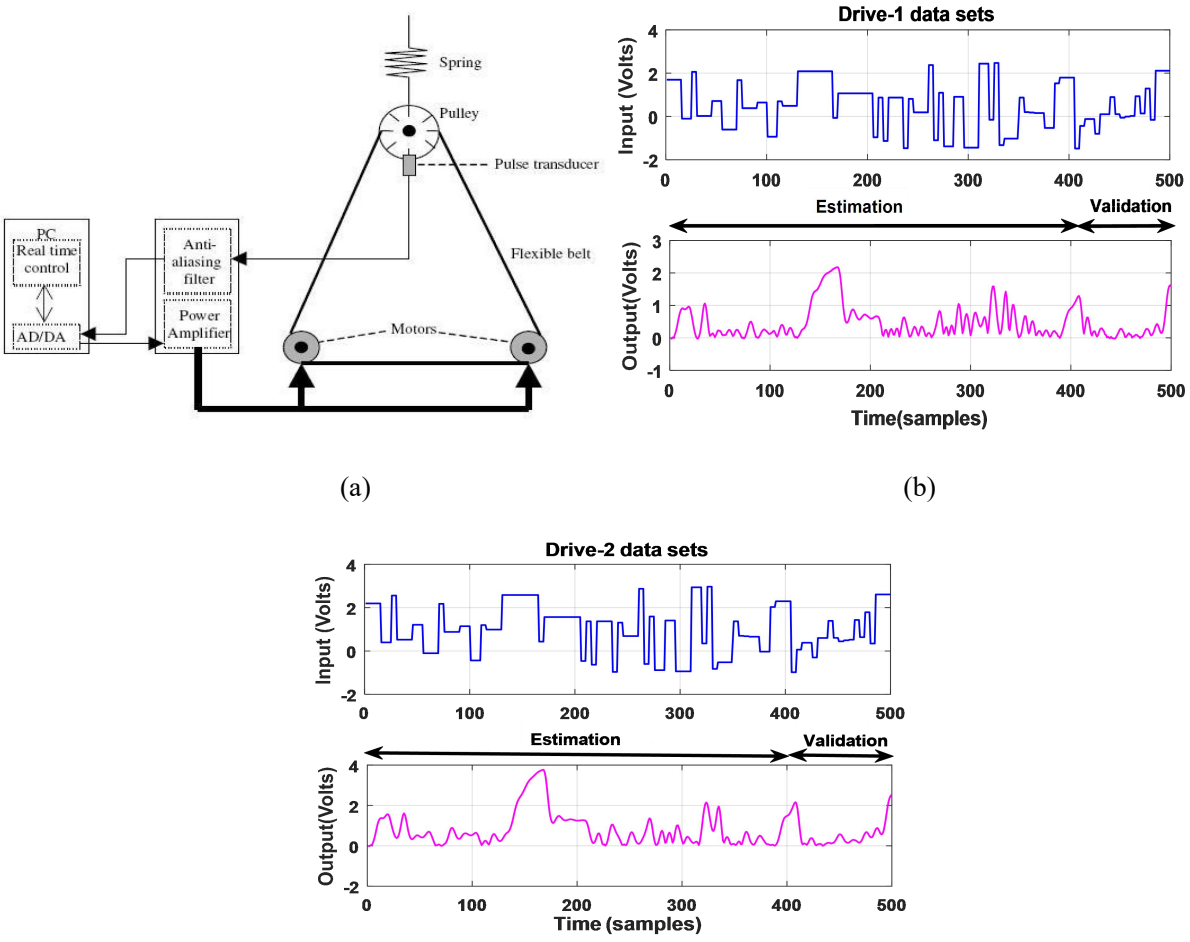

Fig. S7 Identification results of system 4 (coupled electric drive system) using different models based on ROA: (a) laboratory setup; (b) drive-1 I/O datasets; (c) drive-2 I/O datasets

15 Basic details of the CSTR system

CSTR exhibits irreversible exothermic reactions. The schematic view of the CSTR system is shown in Fig. S8a. In CSTR, two chemicals were mixed to generate a product compound 'A' at a concentration $C_A(t)$

and temperature $T(t)$. The coolant flow-rate $q_c(t)$ varies with the temperature, resulting in controlled product concentration. The differential equations of CSTR outputs are given as follows (De Moor, 2004):

$$\dot{C}_A(t) = \left(q/V\right)\left(C_{A0} - C_{A0}(t)\right) - K_0 C_A(t)\exp\left(-E/\mathrm{R}\,\mathrm{T}(t)\right),$$
$$\dot{T}(t) = \left(q/V\right)\left(T_0 - T(t)\right) + K_1 C_A(t)\exp\left(-E/RT(t)\right) + K_2 q_c(t)\left(1-\exp\left(-K_3/q_c(t)\right)\right)\left(T_{c0} - T(t)\right),$$

where q is the process flow rate, C_{A0} and T_0 specify the inlet feed concentration and temperature, respectively, T_{c0} is the coolant temperature, and V , E/R , K_0 , K_1 , K_2 , and K_3 are the thermochemical constants.

The numerical values of the above-said CSTR parameters, constants, and normal functionality conditions are presented in the literature (De Moor, 2004). To model the CSTR using the chosen models, the actual input $q_c(t)$, and output $C_A(t)$ (assume that another output $T(t)$ is constant for a single-input single-output (SISO) system formation (Lightbody and Irwin, 1997; Hafezi and Arefi, 2019; Janjanam et al., 2022b)), datasets are collected from the database for identification of systems (DAISY) (De Moor, 2004), where the authors have picked up the first 1250 samples out of 7500 to reduce CC, which is shown in Fig. S8b. From the total of 1250 samples, the first 1000 samples were allotted for estimation and the rest 250 samples for validation of CSTR.

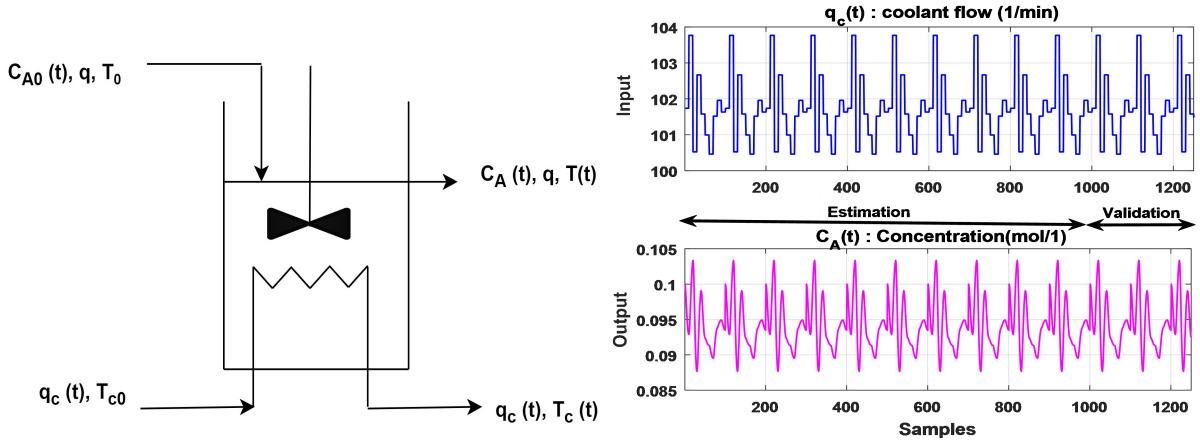

(a) (b)

Fig. S8 CSTR practical plant identification results using ROA: (a) schematic view of CSTR; (b) input and output datasets of CSTR

References

Braik M, Hammouri A, Atwan J, et al., 2022. White shark optimizer: a novel bio-inspired meta-heuristic algorithm for global optimization problems. *Knowl-Based Syst*, 243:108457. https://doi.org/10.1016/j.knosys.2022.108457

De Moor B, 2004. Database for Identification of Systems. https://homes.esat.kuleuven.be/~smc/~daisy/ [Accessed on Nov. 15, 2023].

Jia HM, Peng XX, Lang CB, 2021. Remora optimization algorithm. *Expert Syst Appl*, 185:115665.

Janjanam L, Saha SK, Kar R, et al., 2022a. Hammerstein-Wiener nonlinear system identification by using honey badger algorithm hybridized Sage-Husa adaptive Kalman filter with real-time applications. *AEU Int J Electron Commun*, 151:154218. https://doi.org/10.1016/j.aeue.2022.154218

Janjanam L, Saha SK, Kar R, et al., 2022b. Improving the modelling efficiency of Hammerstein system using Kalman filter and its parameters optimised using social mimic algorithm: application to heating and cascade water tanks. *J Franklin Inst*, 359(3):1239-1273.

Janjanam L, Saha SK, Kar R, et al., 2022c. Wiener model-based system identification using moth flame optimised Kalman filter algorithm. *Signal Image Video Process*, 16(5):1425-1433. https://doi.org/10.1007/s11760-021-02096-w

Hafezi Z, Arefi MM, 2019. Recursive generalized extended least squares and RML algorithms for identification of bilinear systems with ARMA noise. *ISA Trans*, 88:50-61. https://doi.org/10.1016/j.isatra.2018.12.015

Holm S, 1979. A simple sequentially rejective multiple test procedure. *Scand J Stat*, 6(2):65-70.

Lightbody G, Irwin GW, 1997. Nonlinear control structures based on embedded neural system models. *IEEE Trans Neur Netw*, 8(3):553-567. https://doi.org/10.1109/72.572095

Nayak C, Saha SK, Kar R, et al., 2019. An efficient and robust digital fractional order differentiator based ECG pre-processor design for QRS detection. *IEEE Trans Biomed Circ Syst*, 13(4):682-696. https://doi.org/10.1109/TBCAS.2019.2916676

Shadravan S, Naji HR, Bardsiri VK, 2019. The sailfish optimizer: a novel nature-inspired metaheuristic algorithm for solving constrained engineering optimization problems. *Eng Appl Artif Intell*, 80:20-34. https://doi.org/10.1016/j.engappai.2019.01.001

Wigren T, Schoukens J, 2013. Three free data sets for development and benchmarking in nonlinear system identification. European Control Conf, p.2933-2938. https://doi.org/10.23919/ECC.2013.6669201

Yadav S, Saha SK, Kar R, 2023. An application of the Kalman filter for EEG/ERP signal enhancement with the autoregressive realisation. *Biomed Signal Process Contr*, 86:105213. https://doi.org/10.1016/j.bspc.2023.105213